Article

Journal of the Brazilian Chemical Society

https://dx.doi.org/10.21577/0103-5053.20230159

J. Braz. Chem. Soc. **2024**, *35*, 4, e-20230159, 1-16

Reactivity Studies and Synthetic Strategies Towards the Preparation of New Hydrophilic Indirubin-Triazole-Based Compounds

Ana Flávia dos S. Fuzaro,[a] Frederico Henrique do C. Ferreira,[b] Gabriela L. P. Suhett,[a] Luiz Antônio S. Costa,[b] Richard Michael Grazul,[a] Mauro V. de Almeida*,[a] and Eloah P. Ávila*,[a]

[a]*Departamento de Química, Universidade Federal de Juiz de Fora, Campus Martelos, 36036-900 Juiz de Fora-MG, Brazil*

[b]*Núcleo de Estudos em Química Computacional (NEQC), Universidade Federal de Juiz de Fora, Campus Martelos, 36036-900 Juiz de Fora-MG, Brazil*

Indirubin is an isomer of the blue dye indigo. It is widely used in Chinese medicine as part of therapy against many diseases and, thus, its skeleton becomes a promising candidate for new drug prototypes. Since it has low solubility, its properties could be improved through the insertion of hydrophilic and pharmacophoric groups, such as sugars bridged to 1,2,3-triazoles. Here, we report the synthesis of indirubin-based compounds evaluating two different routes: via the aldol condensation reaction of triazole-isatin derivatives with 3-acetoxyindole (pathway A) and reductive coupling of isatin, followed by *N*-propargylation of indirubin. We also performed reactivity studies guided by density functional theory (DFT) calculations (pathway B). As a demonstration, we simulate interactions with the glycogen synthase kinase 3β enzyme, which is associated with neurodegenerative diseases, through both molecular docking and molecular dynamics simulations.

Keywords: indirubin reactivity, isatin functionalization, CuAAC reactions, molecular docking

Introduction

Indirubin (**1**) is an alkaloid belonging to the class of indigoids and is present in plants, such as *Polygonum tinctorium* (Japanese indigo) commonly used in Chinese traditional medicines.[1] Indigoids are recognized by their industrial application as dyes and pigments and, additionally, they present several biological activities such as antiviral, antifungal, antioxidant as well as antiproliferative and antitumoral actions.[2-6] Regarding its anticancer activities, indirubin presents activities against leukemic cells inhibiting cell growth and showing both antineurodegenerative and neuroprotective activities. This compound is recognized due to its ability to inhibit glycogen synthase kinase-3β (GSK-3β) and cyclin-dependent kinases (CDKs) through regulatory action on the striatum nerve that affects the levels of biogenic amines and their regeneration.[7] The neuroprotective properties appear to be mediated by regulation of the activation of mycogenes, responsible for immune and inflammatory responses in the brain, thereby reducing the production of neurotoxic molecules responsible for Alzheimer's and Parkinson's disease.[8]

With regard to its chemical structure, the highly conjugated system results in a nearly planar molecule whose electrons are delocalized (Figure 1).[9]

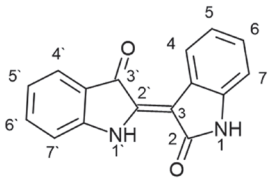

Figure 1. Molecular structure of indirubin (**1**).

Despite presenting promising biological activities, some modifications are needed to overcome problems related to its low solubility and to improve its physicochemical and pharmacological properties. The inclusion of hydrophilic

*e-mail: mauro.almeida@ufjf.br; eloahavila@ice.ufjf.br
Editor handled this article: Brenno A. D. Neto

This manuscript is part of a series of publications in the Journal of the Brazilian Chemical Society by young researchers who work in Brazil or have a solid scientific connection with our country. The JBCS welcomes these young investigators who brighten the future of chemical sciences.

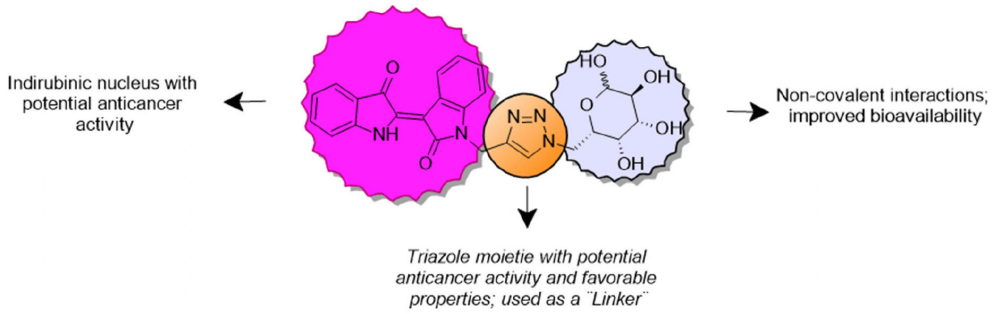

Figure 2. Hydrophilic groups linked to fused triazole-indirubin skeleton.

moieties attached to the original skeleton is one such approach.[10] Recently, Sun *et al.*[11] reported the improvement of anti-proliferative activities in K562 tumor cell of new indirubin-based compounds with oxophylic groups.

Thus, the combination of the indigoid skeleton with carbohydrates along with pharmacophoric groups, such as a 1,2,3-triazole, could outline new approaches for the development of new drugs for anticancer therapies (Figure 2).

The insertion of the triazole ring serves as a hydrogen bond acceptor, which would provide both an improvement in the solubility of the molecule in physiological media and, conceivably, increase or form new interactions between enzymes and proteins from different biological targets.[12] This heterocycle acts as linker of different functional groups in biomolecules, which has been amply demonstrated.[13-15] In addition, the triazole moiety linked with carbohydrates, chalcones, azoles and pyridazines are reported to have antiproliferative activity against various human cell lines.[16-18]

Although functionalized derivatives of indirubin could play a central role in the development of new drug candidates, direct functionalization is still a synthetic challenge due to the intrinsic reactivity of the indirubin nucleus. The functionalization of indirubin by nucleophilic addition often requires alkaline conditions to increase the reactivity of the substrate. This can often compromise the regio- and/or chemoselectivities of subsequent reactions. For example, in the presence of base at elevated temperatures, tryptanthrin (**2**), (Figure 3) is commonly formed after decomposition into isatin (**3**) following by condensation and oxidative rearrangements.[19,20]

As an alternative, we delineated our main strategy starting from the functionalized skeleton (**3**) as a starting material for obtaining indirubin derivatives. Hence, we report a new, selective and fast approach for the insertion of hydrophilic sugar moieties into the indirubin skeleton linked by 1,2,3-triazole groups. Our strategy was centered on the coupling reaction of isatin-triazole-sugar compounds with 3-acetoxyindole via the well-known

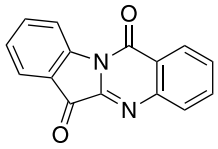

Figure 3. Chemical structure of tryptanthrin (**2**).

aldol condensation reaction (*vide infra*). Additionally, we report the propargylation of the indirubins in basic medium guided by density functional theory (DFT) calculations and experimental data.

Finally, we simulate interactions of these compounds with the GSK-3β enzyme, an important target related to neurodegenerative diseases, through both molecular docking and molecular dynamics aiming to predict their binding structure on the surface of the protein and to evaluate the interaction affinity for the compounds prepared in this paper.

Results and Discussion

Syntheses of triazole-indirubin derivatives

Synthetically, indirubin (**1**) can be obtained through two main pathways, via the aldol condensation reaction between isatin (**3**) and 3-acetoxyindole (**4**), or by reductive dimerization of isatins.[21-23] Of these two methodologies, we evaluated the viability of both pathways employing previously functionalized isatin-triazole-sugars followed by the condensation reaction with 3-acetoxyindole (**4**) (pathway A). We also investigated the reductive coupling of (**3**), propargylation of the resulting indirubin, followed by the copper(I)-catalyzed alkyne-azide cycloaddition (CuAAC) "click chemistry" reaction with the respective sugar azides (pathway B) as an alternative (Scheme 1).[24,25]

The formation of the triazole ring was performed with pyrano and furanoside azide derivatives and *N*-propargyl-isatin as the alkyne sources. The catalytic system consisted of *in situ* reduction of copper II sulfate by sodium ascorbate to generate the reactive Cu-I-acetylide species.[26,27] For pathway A (Scheme 2), the "click" reaction between (**4**)

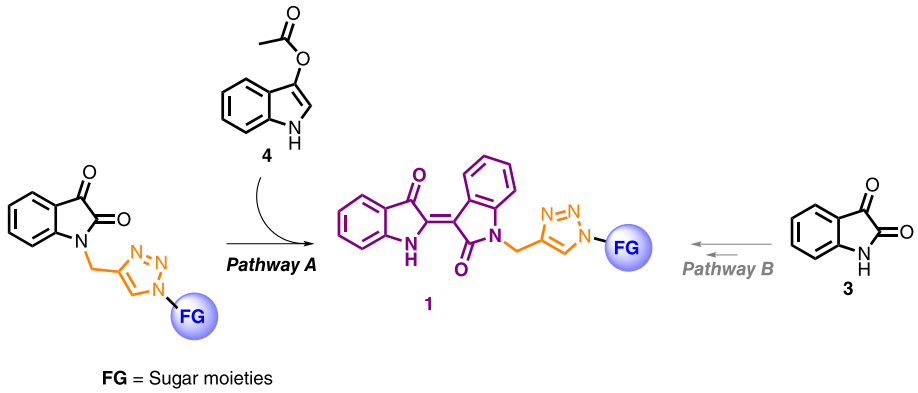

Scheme 1. Strategies for preparation of triazole derivatives linked to hydrophilic moieties.

and the respective organoazides led to the triazole derivatives (**6-8**) in 52 to 76% yields under mild conditions.

The first step was fast, chemoselective and only mild reaction conditions were required to lead to the *N*-functionalized tautomer in 88% yield, even though formation of the *O*-tautomer is possible in solution (see X-ray structure, Figure S1, Supplementary Information (SI) section).[28-30] Subsequently, the aldol condensation reaction between these isatin-triazole intermediates and (**4**) led to the monofunctionalized indirubin-triazoles (**9-11**) in moderate to good yields (Scheme 2, step (*iii*)). It is important to mention that an inert atmosphere is necessary to maintain the chemoselectivity, as the highly reactive indoxyl generated *in situ* is sensitive to oxidative dimerization and, consequently, reacts to form indigo.[31] The described reaction conditions were efficient to obtain the short reaction times and minimize by-product formation.

Finally, hydrophilic derivatives (**12-14**) were obtained after acidic hydrolysis of the isopropylidene protecting groups present in the carbohydrates, with yields ranging from 61 to 99% (Scheme 3). Although it is commonly used trifluoroacetic acid (TFA) in deprotection reactions of carbohydrates, the hydrolysis was not achieved when it was used TFA/H_2O.[32] Then, the reaction carried out after adding two drops of sulfuric acid to access the deprotected carbohydrate derivatives. It is worth mentioning that a mixture of diastereomers is observed when the hemiacetal scaffolding is formed resulting in both α and β anomers, in a 1:1 ratio.

These isatin-triazole derivatives serve as promising starting materials and building blocks for the synthesis of more complex molecules. Hence, we demonstrate as an application, the reductive coupling of compound **15** in order to obtain a *N,N*-difunctionalized adduct (Scheme 4),

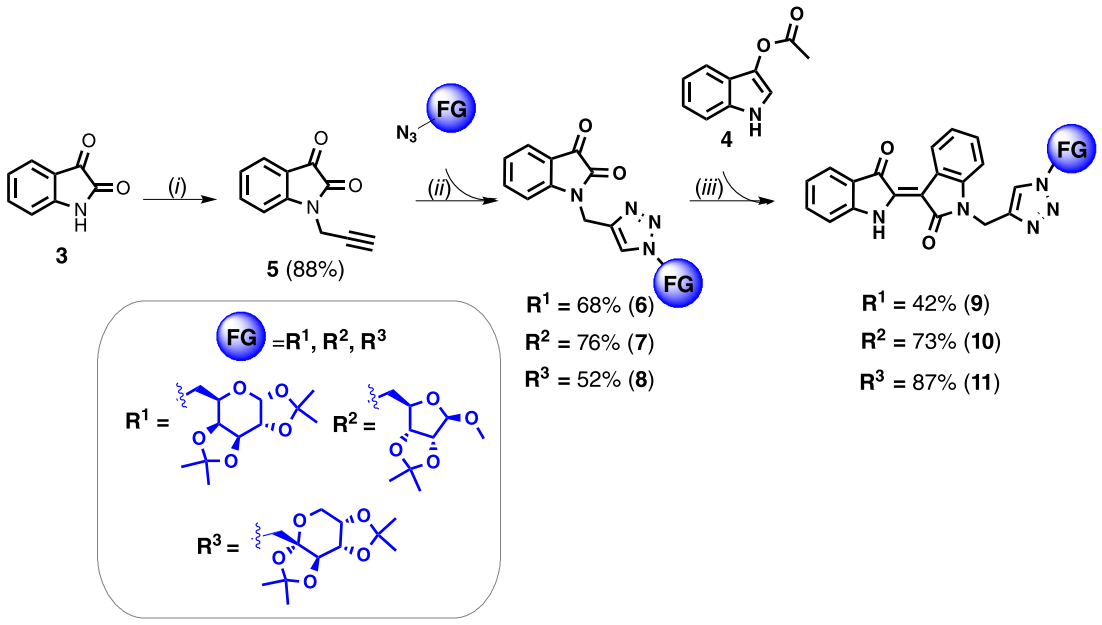

Scheme 2. Synthesis of triazole derivatives through pathway A. (*i*) Propargyl bromide (1.5 eq) K_2CO_3 (1.5 eq), dimethyl sulfoxide (DMSO), room temperature (rt), 1 h (88%); (*ii*) R-N_3 (1.2 eq), DMSO/H_2O, $CuSO_4.5H_2O$ (20 mol%) and sodium ascorbate (20 mol%), rt, 1 h. (*iii*) K_2CO_3 (4.0 eq), MeOH, N_2 atmosphere, rt, 30 min.

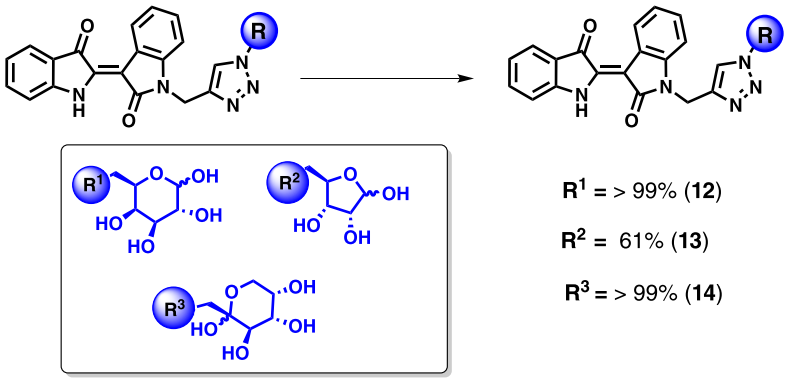

Scheme 3. Hydrolysis of indirubin-triazole derivatives TFA/H_2O 9:1 v/v, 2 drops H_2SO_4, tetrahydrofuran (THF), 60 °C, 24 h.

using the protocol described by Wang *et al.*[21] The resulting product (**16**) was formed as a mixture of diastereomers by the partial reduction process in quantitative yield, and could become a promising strategy for the development of di-functionalized indirubin derivatives.

Therefore, the pathway A can be a strategy to access isatin-triazole-sugars where the aldolic condensation led to only *N*1-monosubstituted indigoids, promising candidates to be applied in a field of medicinal chemistry, as already described by Libnow *et al.*[33] It is important to emphasize that this pathway allows not only monosubstituted derivatives, but it is also a promising path for a double functionalization.

On the other hand, the direct functionalization of the indirubin skeleton was also evaluated (pathway B, Scheme 5), beginning with the reductive coupling reaction of (**3**) followed by propargylation and "click" reactions, respectively. Despite the reductive coupling reaction and click steps being simple, efficient and fast, problems related to the *N*-propargylation step were limiting factors to proceed with this strategy. After several attempts, the loss of selectivity and the formation of degradation products were observed even under mild conditions.

Although we believed that pathway B could be a promising strategy, when we consider the efficiency and how fast the reductive coupling and the click reactions occur, the *N*-functionalization of indirubin requires basic conditions and is a synthetic challenge. Indirubins are not compatible with a basic environment in the presence of atmospheric moisture, or water in the reaction solvents, since under these conditions, a retro-aldol reaction occurs followed by oxidative autocondensation reaction resulting in the formation of tryptanthrin (**2**, Figure S2, SI section) as the major product at elevated temperatures.[20] Therefore, the selective propargylation was not achieved and it compromised this strategy, even under mild conditions. Thus, we decided to investigate the behavior of indirubin in basic medium by control experiments and guided by computational studies through energetic profiles.

Indirubin reactivity under basic environment

The control experiments started with the evaluation of 1.0 equivalent of base and propargyl bromide at low temperature (-10 °C), in an attempt to control the selectivities, but the reaction did not work even after 72 h.

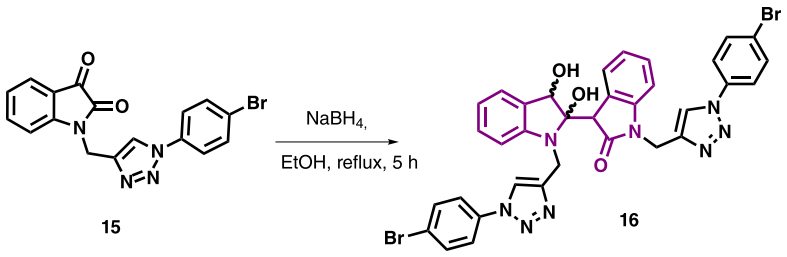

Scheme 4. Partial reductive coupling of triazole-isatin derivative (**15**).

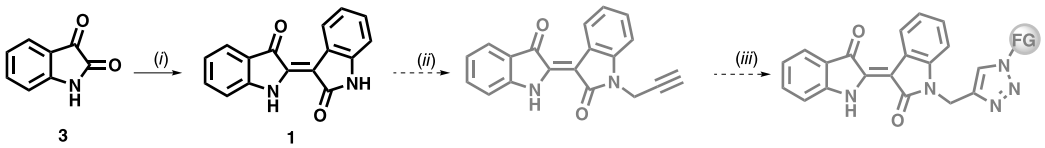

Scheme 5. Pathway B reactions. (*i*) $NaBH_4$, MeOH, 40 min, rt (73%). (*ii*) K_2CO_3 (3.0 eq), propargyl bromide (3.0 eq), KI (cat), DMSO, 72 h.

At room temperature and one equivalent of potassium carbonate (K_2CO_3), the reaction was not accomplished, and only by-products were obtained. Thus, an excess of base is required to improve the reactivity of indirubin, and, in practice, the reaction led to a mixture of functionalized indirubin derivatives, as mono- and dipropargylated ones, as observed in the ^{1}H nuclear magnetic resonance (NMR) spectrum of the reaction crude (Figure 4).

After, we proceeded to evaluate the nucleophilicity of the indirubin skeleton in a basic medium considering the formation of an anionic nucleophile. However, many amides present high pK_a values and carbonate is not a strong base, suggesting that the generation of the anion could be unfeasible and become a limiting factor for the reaction. As there are still no experimental pK_a values for indirubin reported, we assumed that the conjugated base of the indigoid skeleton could be stabilized by resonance since it is highly conjugated.

The control experiments were based on pursuing the identification of indirubin species in basic solution through real-time UV-Vis spectroscopy monitoring. At room temperature, using 1.0, 2.0 and 3.0 equivalents of K_2CO_3, no evidence of formation of anion species was observed since it was only detected a band referring to the π-π* electronic transition at 540 nm, referring to indirubin (Figure 5).

After, the exchanging for a stronger base, as *tert*-butoxide (*t*-BuOK) (3.0 equivalents), the appearance of a redshift band at 700 nm suggested a presence of an anionic species (Figure 6). Although the strength of *t*-BuOK is sufficient to deprotonate indirubin, which would make it ideal for the formation of a nucleophile more effectively, its use is limited by the sensitivity of the indirubin skeleton in strongly basic media.

Then, we outline two proposed mechanisms in which the propargylation reaction would take place, either the neutral pathway or an anionic pathway. In the second case, a small concentration of the deprotonated indirubin could be generated via reaction with K_2CO_3, not detected by UV-Vis spectra.

To delineate a plausible mechanism towards propargylation reaction of indirubin skeleton in basic media, geometry optimizations and harmonic frequency calculations were performed by DFT method using the B3LYP/6-31g(d,p) level of theory and the Polarizable Continuum Model (PCM), using dimethyl sulfoxide (DMSO) as solvent. Higher levels of electronic energies were obtained by single-point energy calculations with the ωB97X-D functional and the 6-311G+(d,p) basis set, which includes diffused functions for all heavy atoms. Solvent effects were included by the solvation model based on density (SMD) method in the single point energies. For details concerning the Cartesian coordinates of the optimized structures (structures I-XL), present in the reaction coordinates, see the Theoretical section of Supplementary Information (SI).

Considering the resonance effects along the indirubin structure, two nucleophilic sites can be generated when both amide (*N*1) or enamine (*N*2) portions are deprotonated (structures **17** and **18**, Scheme 6). As long as *N*1 is arising, the tautomerism could activate the oxygen as a nucleophilic leading to a mixture of **19** and **20**. On the other hand, when the equilibrium of both **17** and **18** is stablished throughout the deprotonation steps, *N2* can act as nucleophile or a

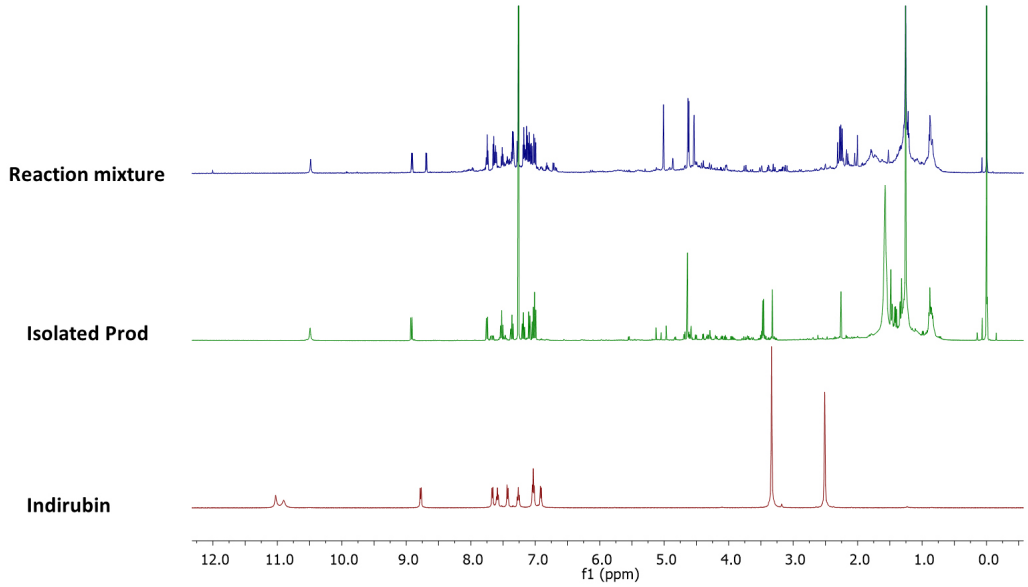

Figure 4. Comparison of ^{1}H NMR spectra of reaction mixture (500 MHz, $CDCl_3$), isolated product (500 MHz, $CDCl_3$) and indirubin (500 MHz, DMSO-d_6).

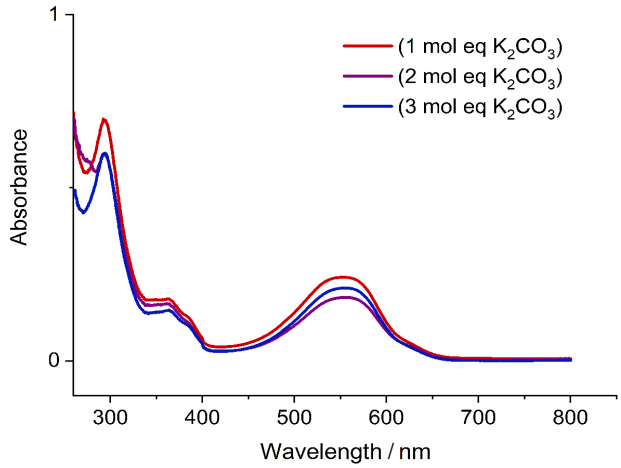

Figure 5. UV-Vis spectra of solution of indirubin with different moieties of K_2CO_3.

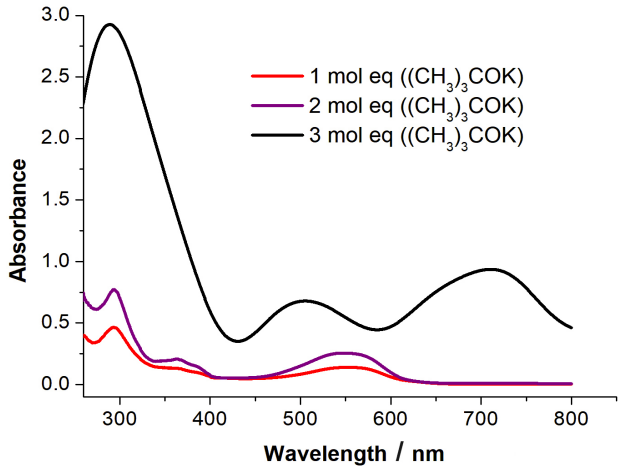

Figure 6. UV-Vis spectra of solution of indirubin with different moieties of *t*-BuOK.

carbanion through resonance effect, leading to **21** and **22**, respectively (Scheme 6).

The equilibrium of both nucleophiles suggests that **17** is the major component being 3.6 kcal mol^{-1} more stable than **18** (Figure 7). Starting from **17**, as the major nucleophile, the *N*1-propargylation process has shown the most kinetically favored, with an energy barrier, $\Delta G^{\ddagger}$, of 21 kcal mol^{-1}, whereas **19** is found as the most stable (–29.3 kcal mol^{-1}). The activation free energy for *O*-propargylation was 4.5 kcal mol^{-1} higher when compared to the most labile one and the product **20** was thermodynamically favored by only 3.9 kcal mol^{-1} in relation to the initial reactants. For **21** and **22** process, they presented the highest energy barriers, 28.7 and 28.1 kcal mol^{-1}, respectively.

When we evaluated a neutral mechanism, it was observed that these processes were kinetically unfavorable for all species (Figure 8), where the barriers ranged from 34.7 to 38.9 kcal mol^{-1}, suggesting that the anionic pathway is more viable and **19** is the major product. However, it is worth to observe that the HBr product can react with K_2CO_3, making the process thermodynamically viable, although kinetically unfeasible.

A second propargylation reaction could take place into *N*2 or *C*3 sites while the more stable monopropargylated product, **19**, is generated. It is noteworthy that functionalization in *N*2 is favorable starting from previously *N*1-functionalized indirubin, because the calculated $\Delta G^{\ddagger}$ = 21.0 kcal mol^{-1} (see Figure 9).

These results can explain the experimental results, in which three signals ranging from 4.50 to 4.62 ppm (Figure 10), characteristic of *N*-methylene hydrogen atoms, suggesting a mixture of *N*1-propargyl and *N*1-*N*2-dipropargyl in a ratio of 1:1.

Moreover, the *N*2-propargylation barrier energy is lower in 4 kcal mol^{-1} in relation to *C*-propargylation. Again, the neutral pathway proved to be highly energetic and kinetically unfeasible (Figure 11).

Finally, when we compare the reactivity of compounds **3** and **1** under propargylation reactions in basic medium, **3** showed to be the most selective. According to the energy profile of both tautomers, the reaction in *N* as nucleophile presented $\Delta G^{\ddagger}$ of 21.7 against 26.8 kcal mol^{-1} of the tautomer *O*. Furthermore, the *O*-functionalized product has a slightly negative ΔG by

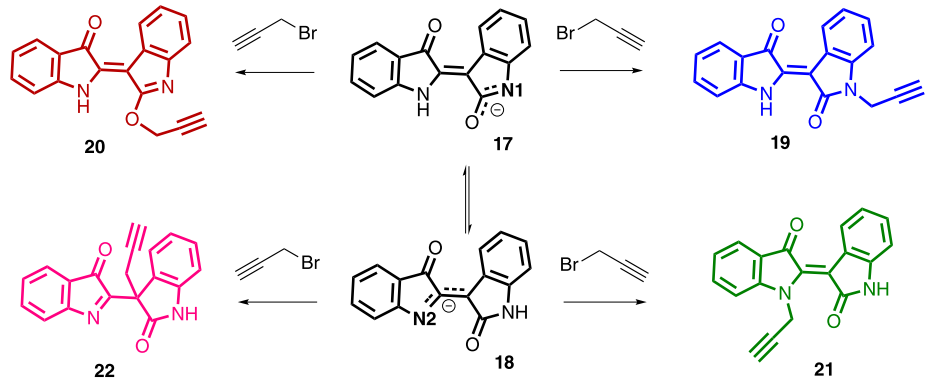

Scheme 6. Different possible isomers towards propargylation reaction: *N*1-propargyl (blue), *O*-propargyl (red), *C*3-propargyl (pink) and *N*2-propargyl (green).

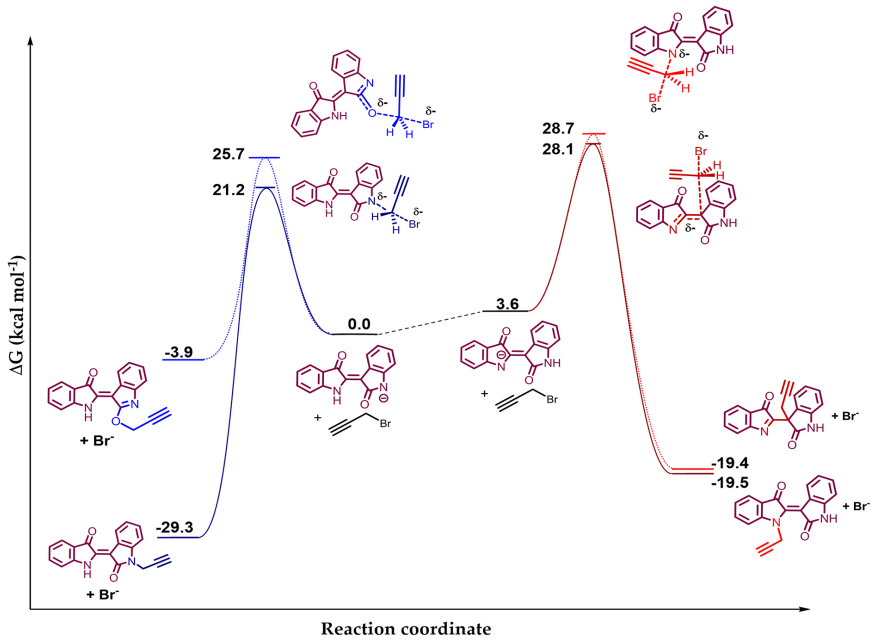

Figure 7. Free energy profile (ΔG) of indirubin monopropargylation reaction through anionic pathway. Units in kcal mol^{-1}, the standard state of 1 mol L^{-1} for all species, 298 K. The imaginary frequencies for transition states (TS) were 380i, 390i, 377i and 332i cm^{-1} for **19**, **20**, **21** and **28**, respectively.

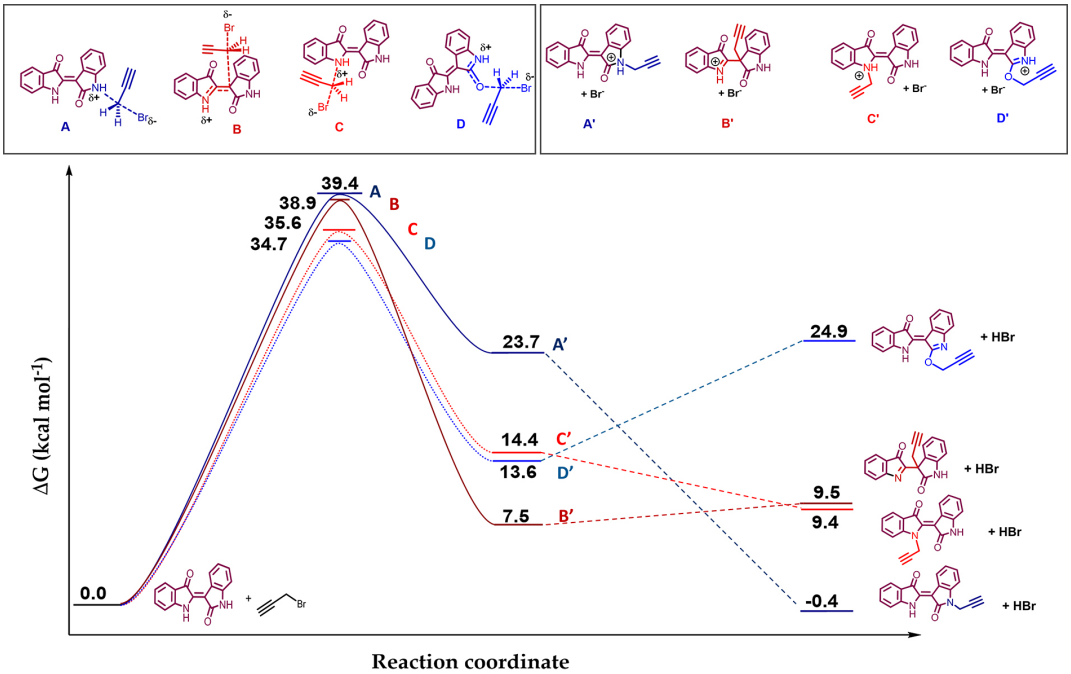

Figure 8. Free energy profile (ΔG) of indirubin monopropargylation reaction through neutral pathway. Units in kcal mol^{-1}, the standard state of 1 mol L^{-1} for all species, 298 K. The imaginary frequencies for TS were 412i, 410i, 349i and 405i cm^{-1} for *N1*, *O*, *C* and *N*2, respectively.

0.4 kcal mol^{-1}, suggesting that only the *N*-functionalized product should be observed.[30]

These results suggest that the theoretical data are in good agreement with the experimental observations and emphasize the importance of pathway A as a viable route in the synthesis of triazole derivatives of indirubin. Unselective reactions attempting the dipropargylation of tautomeric anions compromise chemoselectivity and may be a limiting factor to proceed in the direct functionalization of indirubin derivatives using this methodology.

Molecular docking and molecular dynamics

With the aim to show the possible interactions with promising biological targets, we have evaluated the binding energies with the GSK-3β enzyme responsible for the

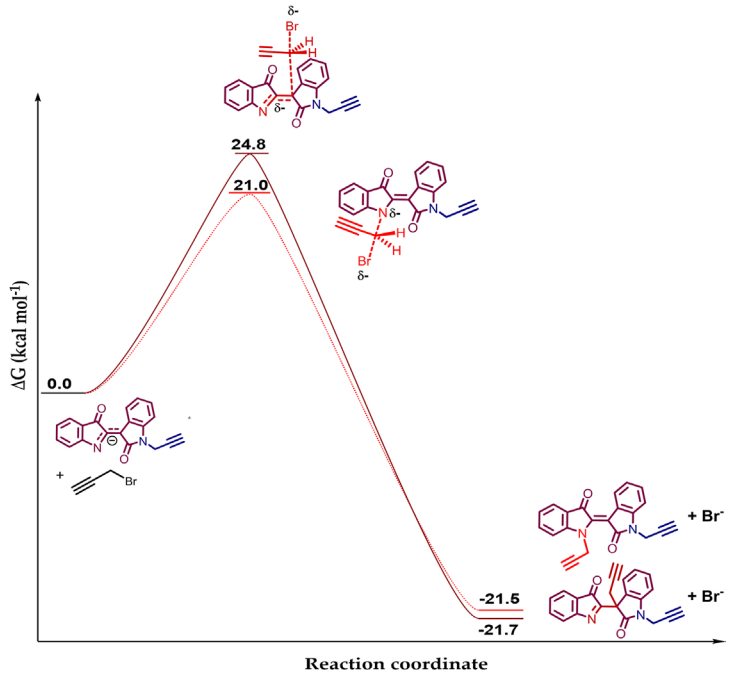

Figure 9. Free energy profile (ΔG) of anionic pathway for a second propargylation reaction involving *N*1-propargyl-indirubin. Units in kcal mol^{-1}, standard state of 1 mol L^{-1} for all species, 298 K. The imaginary frequencies for TS were 339i and 382i cm^{-1} i for *N*2 and *C* propargylation, respectively.

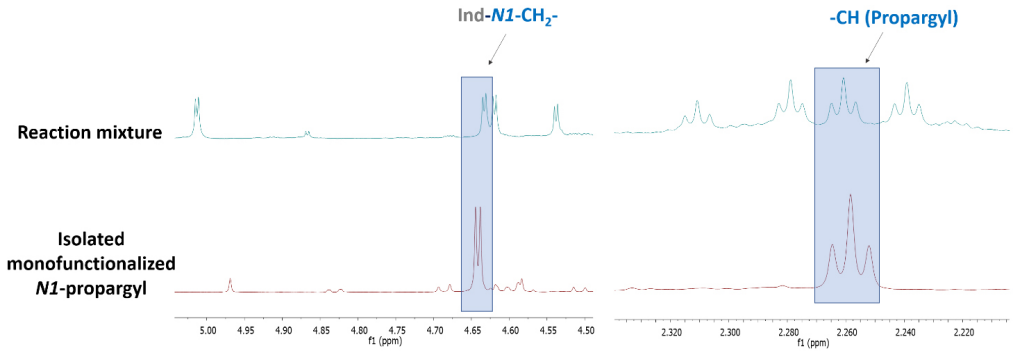

Figure 10. Expansion area of the ^{1}H NMR spectra of methylene and methine hydrogen atoms of reaction mixture and isolated product.

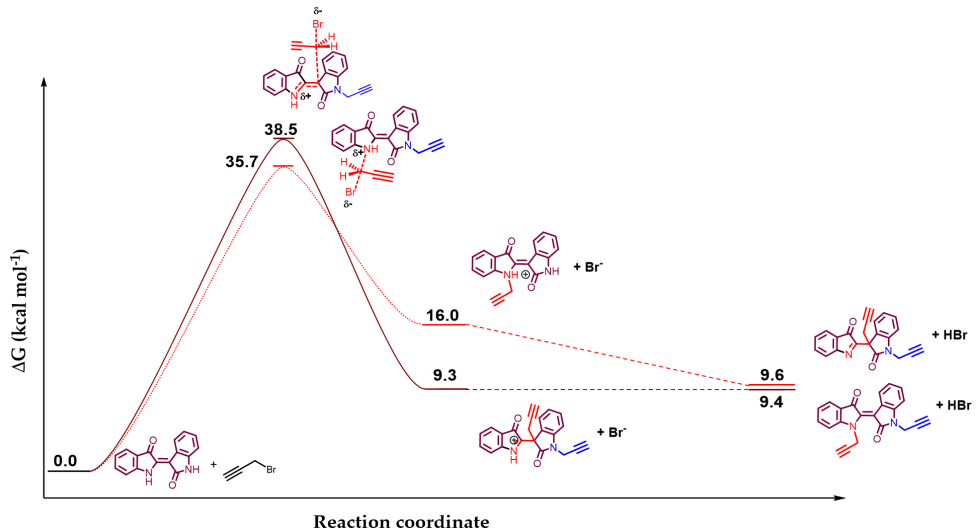

Figure 11. Free energy profile (ΔG) of neutral pathway for dipropargylation reaction of *N*1-propargyl-indirubin. Units in kcal mol^{-1}, the standard state of 1 mol L^{-1} for all species, 298 K. The imaginary frequencies for TS were 391i and 410i cm^{-1} i for *N*2 and *C* propargylation, respectively.

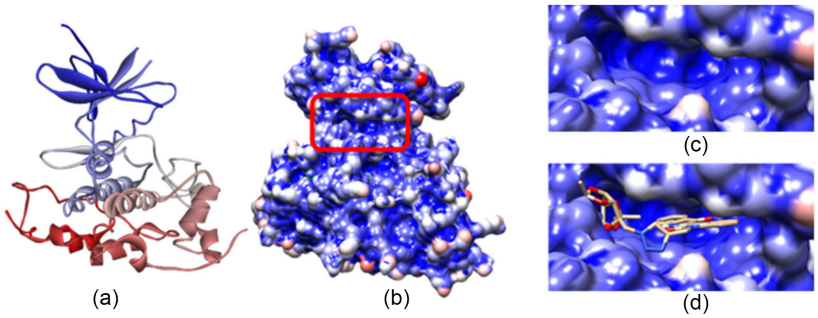

Figure 12. (a) Representation of GSK-β colored from *C*-terminal to *N*-terminal (from blue to red), (b) solid representation of the protein highlighting the active site cavity which is zoomed in (c) and (d) the complex between the protein and compound **9** having the lowest binding energy obtained from the docking analysis. Non-polar hydrogens are omitted for clarity. In the ligand, atoms are colored by element: white polar hydrogen, blue: nitrogen, red oxygen and brown carbon.

regulation of serine-threonine kinase, through molecular docking and molecular dynamics. GSK-3β (Figure 12) plays an important role in the phosphorylation of a wide range of biological substrates with widely varying targets.[1,34-37]

Initially, the GSK-3β structure taken from Protein Data Bank (PDB) under the code 1Q41 had the residues renumbered by pdbtoamber script for the sake of clarity. The references between old and new sequences are shown in SI section. CHIR-98014 and bio-acetoxime were employed as reference ligands based on the literature.[38]

As described by Dan *et al.*,[24] the reference molecule CHIR-98014 has five stabilizing hydrogen bonds with the GSK-3β enzyme along residues Ile62, Tr138, Val135 and Gln185, since the structure has several H-bond acceptor sites, such as the ethylenediamine moiety, and also H-bond donors, situated proximally to the pyrimidine and diazole heterocycles.

In relation to the second reference ligand, bio-acetoxime, it contains the indirubin core and is known to be a selective inhibitor of GSK-3α/β (half maximal inhibitory concentration (IC_{50}) of 10 nM) with three hydrogen bonds to the enzyme.[24]

Based on the docking simulations, the binding energies for the best scoring interaction mode along with the interaction constant calculated by the software were obtained (Table 1). Comparison of the synthesized molecules and the respective starting materials showed that the starting triazoles (**6**-**8**) were less stable than the bio-acetoxime ligand, with a score ΔG of 0.91, 1.59 and 0.95 kcal mol^{-1}, respectively. However, when incorporated into the indirubin skeleton, the scored stabilization energy was lower (ΔG of –2.32, –0.62 and –1.75 kcal mol^{-1} for compounds **10**, **11** and **12**, respectively. This suggests that the chiral carbohydrate moieties, protected as their isopropylidene derivatives, confer rigidity. In contrast, with the free hydroxyl groups, these indirubin-based compounds showed lower stabilities (a score of 0.77 against –2.32 for **9** and **12**-α, respectively).[39]

Table 1. Docking binding energies (kcal mol^{-1}) obtained for the compounds in comparison to the references along with its estimated inhibition constant K_i (in 298.15 K)

Compound	Docking binding energies / (kcal mol^{-1})	K_i / nM
	Best score	
6	–9.17	190.98
7	–8.49	594.92
8	–9.13	204.28
9	–12.4	817.11 pM
10	–10.7	14.27
11	–11.83	2.14
12-α	–9.31	149.13
12-β	–10.01	46.21
13-α	–10.65	15.68
14-β	–9.83	62.76
14-α	–10.66	15.38
14-β	–10.09	40.1
Bio-acetoxime	**–10.08**	**40.63**
CHIR-98014	**–8.57**	**520.14**

As for the ligand CHIR, a less rigid structure, almost all the molecules were more active and compound **8** presented almost 4 kcal of extra stability.

According to the docking energies, the most active compound, **9**, has main interactions to the enzyme via van der Waals throughout the conjugated system of the indirubin scaffold (Figure 13). The isopropylidene groups show p-alkyl interactions with Leu148, Val95 and Tyr94. Similarly, **10** presented energies proximate to **8**, since both present the rigid pyranose skeleton (–11.3 kcal mol^{-1}).

Finally, considering the anomeric, hydrophylic indirubin-based compounds, the β-diastereomer was slightly stable than the α anomer. The α-compounds **12** and **13**, in a similar way, presented similar energy values and more stability than their β counterparts.

The three best compounds found in the docking

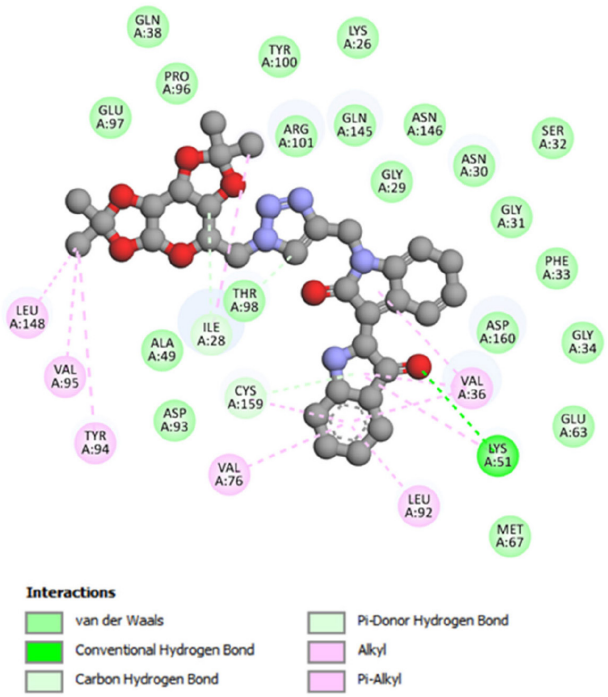

Figure 13. Ligand interactions in the active site of the protein GSK-3β.

simulations, compounds **9**, **10** and **11**, were subjected to molecular dynamics simulations. In general, all complexes reduced the root mean square deviation (RMSD) of the active site of the protein, whose mean accounted for 2.33 ± 0.23 Å in compound **9**, 2.09 ± 0.13 Å in compound **10** and 2.07 ± 0.21 Å in compound **11**. In other words, a reduction in the degree of atomic deviation may imply a constant interaction of the studied compounds, which reduces the freedom of the atoms in the residues in the active site. The very same tendency was observed when the surface accessible solvent area (SASA) was evaluated, which describes the behavior regarding the availability of the protein surface to the solvent, and thus, to other solutes and ligands. Compound **9** was the one that most reduced the active site available surface (with a mean value of 6096.76 ± 218.13 Å^2), followed by compounds **11** (6108.24 ± 227.95 Å^2) and **10** (6272.39 ± 219.96 Å^2). In general, all molecules reduced both atomic deviation (2.55 ± 0.16 Å) and surface accessible solvent area (6619.25 ± 212.01 Å^2) in comparison to the reference trajectory. The graphical data are shown in Figures 14a and 14b.

Conclusions

In summary, we report the synthesis of 13 novel compounds, of which 7 contain indirubin- linked by 1,2,3-triazoles to sugar moieties. The compounds were obtained in moderate to high yields, under mild reaction conditions and short steps. Compounds **12-14** were obtained as a mixture of diastereomers; derivatives of the α and β sugar anomers. A loss of chemoselectivity was observed when an excess of both base and propargyl bromide were employed in the *N*-propargylation reaction of indirubin, this being the limiting factor to continue on this route. The quantum mechanics (QM) analysis of the reactivity of indirubin skeleton showed a good agreement with experimental results. It is suggested that the anionic pathway is the most viable for propargylation reactions, although the process is slower for the formation of the nucleophile because the carbonate is a weak base. Finally, the molecular docking simulations showed that compound **9**, presented better interactions with the target than the reference compounds investigated, even the bio-acetoxime that presents the same scaffolding.

Therefore, *N*1-propargylation reactions seem to be more labile when compared to *O* ones through an anionic nucleophile. Furthermore, the barrier for the second reaction in *N*2 was lower when compared to the C-3 position. According to the experimental results, the ^{1}H NMR spectrum of the reaction crude, the methylene

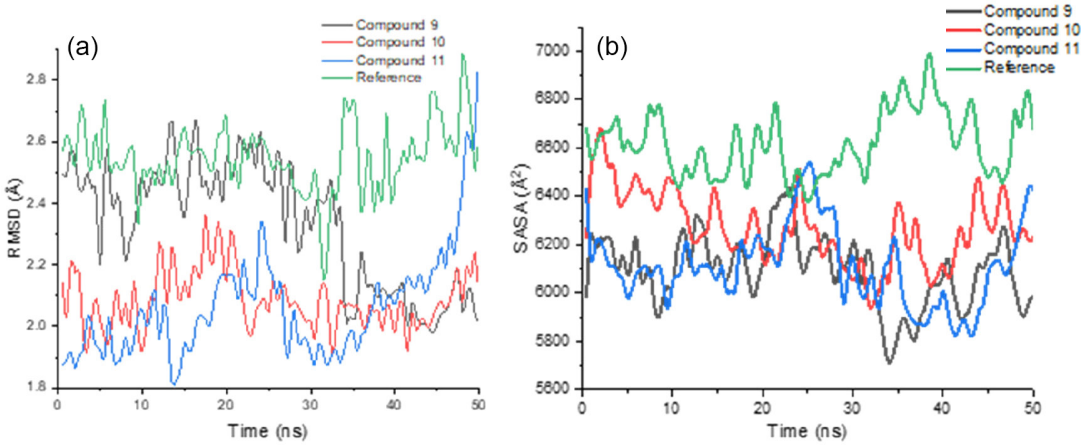

Figure 14. (a) RMSD analysis for the compounds **9**, **10** and **11** complexes with ligand (GSK-3) and (b) SASA analysis with respect to the same systems.

signals indicate a mixture of mono *N*1 and *N*1,*N*2-difunctionalized in a ratio of 1:1.

Experimental

General procedures

The starting materials isatin, D-galactose, D-ribose and D-fructose were obtained from commercial sources. Oxidation sensitive reactions were performed under an atmosphere of N_2. The reactions were monitored by thin layer chromatography (TLC) using silica gel pre-coated plates (Macherey-Nagel, Düren, Germany), and visualized by a UV lamp (254 nm), iodine (I_2) and a solution of 80% ethanol/H_2SO_4. Flash column chromatography was performed on 230-400 mesh silica gel (Saint Louis, USA) using hexane (Êxodo Científica, Sumaré, Brazil) and ethyl acetate (Synth, Diadema, Brazil) mixture as eluent. Yields refer to chromatographically purified and spectroscopically pure compounds.

The NMR spectra were registered on a Bruker Avance III spectrometer (Bremen, Germany), operating at 600, 500, and 400 MHz for ^{1}H and at 151, 125 and 101 MHz for ^{13}C, with $CDCl_3$ and DMSO-d_6 as solvents. Chemical shifts for ^{1}H and ^{13}C NMR were reported as δ (parts *per* million, ppm) relative to the signals of the residual solvent peaks. NMR chemical shifts are reported employing the following peak abbreviation pattern: s, singlet; d, duplet; t, triplet; q, quartet; dd, double doublet; td, triplet doublet; s, septet; m, multiplet. The values of coupling constants (*J*) are in Hz and the ^{13}C NMR were proton decoupled. The infrared (IR) spectra were acquired on a Bruker Vertex 70, Hyperion spectrometer equipped with a diamond point, with resolution of 4 cm^{-1} and a spectral range from 400 to 4000 cm^{-1}.

N-Propargyl-isatin derivative (compound **5**)

To a solution of isatin (5.0 mmol) in DMSO (10 mL) it was added potassium carbonate (5.0 mmol) and stirred at room temperature for 10 min. Propargyl bromide 1 eq was then added and the reaction mixture was kept under stirring for 1 h. The reaction mixture was then quenched with the addition of water (20 mL). The crude mixture was extracted with EtOAc (3 × 50 mL). The organic extract was dried with anhydrous sodium sulfate and solvent excess was evaporated under reduced pressure. The product was obtained after purification by column chromatography (gradient elution: ethyl acetate/hexane). The spectral data is in accordance with that described in the literature for compound **5**.[30]

1-(2-Propynyl)-1*H*-indole-2,3-dione (**5**)

IR (ATR) ν / cm^{-1} 3262, 2355, 1747, 1619, 1463, 1352, 1201, 1099, 1038, 936, 768, 692, 483; ^{1}H NMR (500 MHz, $CDCl_3$) δ 7.68-7.63 (m, 2H, H-7 and H-9), 7.19 (tdd, *J* 7.6, 2.3, 0.8 Hz, 1H, H-10), 7.15 (dd, *J* 7.9, 0.7 Hz, 1H, H-8), 4.55 (t, *J* 2.4 Hz, 2H, H-3 and H-3'), 2.33 (t, *J* 2.5 Hz, 1H, H-1); ^{13}C NMR (126 MHz, $CDCl_3$) δ 182.7, 157.7, 149.7, 138.6, 125.5, 124.3, 117.8, 111.2, 75.8, 73.5, 29.5.

General preparation of organoazides

The alkyl azides were obtained following literature protocols[40,41] in three steps: protection, iodination and azidation. The aryl azide was obtained from the diazonium salt of 4-bromoaniline.[41]

Isatin-triazole derivatives (compounds **6-8** and **15**)

To a solution of the organic azide (0.7 mmol, 1.2 eq) in DMSO (2 mL), it was added *N*-propargyl isatin (0.58 mmol, 1.0 eq), an aqueous solution of 20 mol% $CuSO_4.5H_2O$ and 20 mol% sodium ascorbate (NaAsc). The solution was stirred at room temperature for one hour and monitored by TLC (7:3 hexane/ethyl acetate). Subsequently, the crude reaction mixture was added to ice water and the resulting solid was filtered under vacuum. The resulting reaction mixture was extracted with ethyl acetate (3 × 30 mL) and solvent excess was evaporated under reduced pressure. All solid obtained was purified by column chromatography (6:4 hexane/ethyl acetate).

1-((1-(((3a*R*,5*R*,5a*S*,8a*S*,8b*R*)-2,2,7,7-Tetramethyltetrahydro-5*H*-bis([1,3]dioxolo)[4,5-*b*:4',5'-*d*]pyran-5-yl)methyl)-1*H*-1,2,3-triazol-4-yl)methyl)indoline-2,3-dione (**6**)

IR (ATR) ν /cm^{-1} 2989, 2102, 1732, 1612, 1468, 1360, 1302, 1246, 1217, 1169, 1113, 1067, 1003, 906, 858, 819, 769, 686, 472; ^{1}H NMR (600 MHz, $CDCl_3$) δ 7.78 (s, 1H, H-10), 7.58-7.54 (m, 2H, H-4 and H-6), 7.27 (d, $^3J_{7,6}$ 5.0 Hz, 1H, H-7), 7.09 (t, $^3J_{5,4}$ 7.5 Hz, $^3J_{5,6}$ 7.5 Hz, 1H, H-5), 5.46 (d, $^3J_{1',2'}$ 4.9 Hz, 1H, H-1'), 5.06 (d, $^2J_{8,8'}$ 15.6 Hz, 1H, H-8), 4.98 (d, $^2J_{8',8}$ 15.6 Hz, 1H, H-8'), 4.61 (dd, $^3J_{3',4'}$ 6.5, $^3J_{3',2'}$ 2.1 Hz, 1H, H-3'), 4.57 (dd, $^2J_{6',6''}$ 11.9, $^3J_{6',5'}$ 3.3 Hz, 1H, H-6'), 4.41 (dd, $^2J_{6'',6'}$ 11.9, $^3J_{6'',5'}$ 7.1 Hz, 1H, H-6''), 4.30 (dd, $^3J_{2',1'}$ 4.9, $^3J_{2',3'}$ 2.1 Hz, 1H, H-2'), 4.14 (dd, $^3J_{4',3'}$ 6.5, $^3J_{4',5'}$ 1.5 Hz, 1H, H-4'), 4.11 (ddd, $^3J_{5',6''}$ 7.15, $^3J_{5',6'}$ 3.2, $^3J_{5',4'}$ 1.6 Hz, 1H, H-5'), 1.46 (s, 3H, -CH_3), 1.33 (s, 3H, -CH_3), 1.31 (s, 3H, -CH_3), 1.26 (s, 3H, -CH_3); ^{13}C NMR (151 MHz, $CDCl_3$) δ 183.3, 158.0, 150.5, 141.5, 138.7, 125.4, 124.4, 124.0, 117.7, 111.7, 110.1, 109.2, 96.3, 71.2, 70.9, 70.4, 67.2, 50.8, 35.6, 26.0, 25.9, 25.0, 24.5; HR-MS (Fourier transform mass

spectrometry (FTMS) + pESI) *m/z*, calcd. for $C_{23}H_{27}N_4O_7$ $[M]^+$: 471.1874, found: 471.1879.

1-((1-(((3a*R*,4*R*,6*R*,6a*R*)-6-Methoxy-2,2-dimethyltetrahydrofuro[3,4-*d*][1,3]dioxol-4-yl)methyl)-1*H*-1,2,3-triazol-4-yl)methyl)indoline-2,3-dione (**7**)

IR (ATR) ν /cm^{-1} 2954, 2834, 1771, 1622, 1474, 1439, 1358, 1195, 1085, 1056, 963, 887, 765, 474; ^{1}H NMR (500 MHz, $CDCl_3$) δ 7.73 (s, 1H, H-10), 7.59-7.56 (m, 2H, H-4 and H-6), 7.32 (d, $^3J_{7,6}$ 10 Hz, 1H, H-7), 7.10 (t, $^3J_{5,4}$ 10, $^3J_{5,6}$ 10 Hz, 1H, H-5), 5.02 (s, 2H, H-8 and H-8'), 4.98 (s, 1H, H-1'), 4.72 (d, $^3J_{2',3'}$ 5 Hz, 1H, H-2'), 4.62 (d, $^3J_{3',2'}$ 5 Hz, 1H, H-3'), 4.55-4.50 (m, 2H, H-5' and H-5''), 4.39 (td, $^3J_{4',5'}$ 11.4 Hz, $^3J_{4',5''}$ 11.4 Hz, *J* 7.0 Hz, 1H, H-4'), 3.34 (s, 3H, -OCH_3), 1.43 (s, 3H, -CH_3), 1.28 (s, 3H, -CH_3); ^{13}C NMR (126 MHz, $CDCl_3$) δ 183.2, 158.1, 150.3, 142.0, 138.7, 125.4, 124.1, 123.7, 117.6, 113.1, 111.6, 110.1, 85.2, 82.0, 55.6, 53.7, 41.0, 35.5, 26.5, 25.0.

1-((1-(((3a*S*,5a*S*,8a*S*,8b*R*)-2,2,7,7-Tetramethyltetrahydro-3a*H*-bis([1,3]dioxolo)[4,5-*b*:4',5'-*d*]pyran-3a-yl)methyl)-1*H*-1,2,3-triazol-4-yl)methyl)indoline-2,3-dione (**8**)

IR (ATR) ν / cm^{-1} 2930, 1733, 1608, 1465, 1375, 1218, 1116, 1059, 1009, 864, 759, 471; ^{1}H NMR (600 MHz, $CDCl_3$) δ 7.75 (s, 1H, H-10), 7.56 (m, 2H, H-4 and H-6), 7.32 (d, $^3J_{7,6}$ 5.0 Hz, 1H, H-7), 7.10 (t, $^3J_{5,4}$ 5.0, $^3J_{5,6}$ 5.0 Hz, 1H, H-5),), 5.06 (d, $^2J_{8,8'}$ 15.0 Hz, 1H, H-8), 4.99 (d, $^2J_{8',8}$ 15.0 Hz, 1H, H-8'), 4.69 (d, $^2J_{6',6''}$ 14.4 Hz, 1H, H-6'), 4.61 (dd, $^3J_{3',4'}$ 7.7, $^3J_{3',2'}$ 2.7 Hz, 1H, H-3'), 4.50 (d, $^2J_{6'',6'}$ 14.4 Hz, 1H, H-6''), 4.36 (d, $^3J_{2',3'}$ 2.7 Hz, 1H, H-2'), 4.22 (d, $^3J_{4',3'}$ 7.7 Hz, 1H, H-4'), 3.87 (dd, $^2J_{5',5''}$ 12.9 Hz, $^3J_{5',4'}$ 1.6 Hz, 1H, H-5'), 3.76 (d, $^2J_{5'',5'}$ 13.0 Hz, 1H, H-5''), 1.49 (s, 3H, -CH_3), 1.42 (s, 3H, -CH_3), 1.35 (s, 3H, -CH_3), 0.65 (s, 3H, -CH_3); ^{13}C NMR (151 MHz, $CDCl_3$) δ 183.2, 158.0, 150.4, 141.6, 138.7 125.8, 125.4, 124.2, 117.6, 111.8, 109.6, 109.5, 100.7, 70.8, 70.7, 70.1, 62.0, 55.4, 35.5, 26.5, 26.1, 24.3, 24.1; HR-MS (FTMS + pESI) *m/z*, calcd. for $C_{20}H_{23}N_4O_6$ $[M]^+$: 471.1874, found: 471.1879.

1-[1-(4-Bromo-phenyl)-1*H*-[1,2,3]triazol-4-ylmethyl]-1*H*-indole-2,3-dione (**15**)

^{1}H NMR (500 MHz, $CDCl_3$) δ 8.05 (s, 1H), 7.66-7.64 (m, 2H), 7.60 (t, *J* 7.2 Hz, 4H), 7.36 (d, *J* 8.6 Hz, 1H), 7.14 (t, *J* 7.5 Hz, 1H), 5.10 (s, 2H); ^{13}C NMR (126 MHz, $CDCl_3$) δ 161.8, 159.9, 146.4, 134.7, 132.8, 124.0, 120.6, 52.0, 40.7.

General procedure for indirubin-triazole derivatives (compounds **9**-**11**)

In a round bottom flask containing a methanolic solution of isatin triazole (0.2 mmol, 1.0 eq, 2 mL) under an inert atmosphere, it was added K_2CO_3 (0.772 mmol, 4.0 eq) and 3-acetoxyindole (0.193 mmol, 1.0 eq). The solution was stirred for 35 min, and the consumption of the starting material was verified by TLC (7:3 hexane/ethyl acetate) and the color of the reaction medium changed from orange to violet. The solids were solubilized in dichloromethane, neutralized by Amberlite IR 120 and then filtered. The organic phase was dried under reduced pressure and the solids obtained were purified by gradient column chromatography (hexane/ethyl acetate 7:3→ethyl acetate/ethanol 9:1).

((*Z*)-1'-((1-(((3a*R*,5*R*,5a*S*,8a*S*,8b*R*)-2,2,7,7-Tetramethyltetrahydro-5*H*-bis([1,3]dioxolo)[4,5-*b*:4',5'-d]pyran-5-yl)methyl)-1*H*-1,2,3-triazol-4-yl)methyl)-[2,3'-biindolinylidene]-2',3-dione (**9**)

IR (ATR) ν / cm^{-1} 3420, 3294, 2985, 1715, 1666, 1593, 1470, 1356, 1172, 1082, 1009, 755, 451; ^{1}H NMR (500 MHz, $CDCl_3$) δ 10.55 (s, 1H, H-1'), 8.87 (d, *J* 7.7 Hz, 1H, H-4), 7.74 (d, *J* 7.6 Hz, 1H), 7.67 (s, 1H), 7.51 (td, *J* 8.1, 1.2 Hz, 1H), 7.28 (dd, *J* 7.7, 1.1 Hz, 1H), 7.10 (dd, *J* 10.4, 4.2 Hz, 2H), 7.02 (td, *J* 7.6, 0.5 Hz, 1H), 6.99 (d, *J* 8.0 Hz, 1H), 5.45 (d,$^3J_{1'',2''}$ 4.9 Hz, 1H, H-1''), 5.20 (d, $^2J_{8,8'}$ 15.7 Hz, 1H, H-8), 5.11 (d, $^3J_{8',8}$ 15.7 Hz, 1H, H-8'), 4.59 (dd, $^3J_{3'',4''}$ 7.6, $^3J_{3'',4''}$ 2.5 Hz, 1H, H-3''), 4.55 (dd, $^2J_{6'',6'''}$ 14.3, $^3J_{6'',5''}$ 3.9 Hz, 1H, H-6''), 4.38 (dd, $^2J_{6''',6''}$ 14.3, $^3J_{6''',5''}$ 8.4 Hz, 1H, H-6''), 4.28 (dd, $^3J_{2'',1''}$ 4.9, $^3J_{2'',3''}$ 2.6 Hz, 1H, H-2''), 4.13 (m, 2H, H-4'' and H-5''), 1.44 (s, 3H, -CH_3), 1.30 (s, 3H, -CH_3), 1.29 (s, 3H, -CH_3), 1.25 (s, 3H, -CH_3); ^{13}C NMR (126 MHz, $CDCl_3$) δ 188.2, 170.4, 151.6, 142.7, 140.0, 139.4, 137.0, 129.4, 125.5, 125.3, 123.7, 122.8, 121.7, 121.1, 120.1, 109.9, 109.1, 109.0, 106.4, 96.2, 71.1, 70.7, 70.3, 67.1, 50.6, 35.4, 29.7, 25.9, 25. 8, 24.9, 24.3.

(*Z*)-1'-((1-(((3a*R*,4*R*,6*R*,6a*R*)-6-Methoxy-2,2-dimethyltetrahydrofuro[3,4-*d*][1,3]dioxol-4-yl)methyl)-1*H*-1,2,3-triazol-4-yl)methyl)-[2,3'-biindolinylidene]-2',3-dione (**10**)

IR (ATR) ν / cm^{-1} 3317, 2930, 1715, 1651, 1631, 1585, 1465, 1358, 1317, 1166, 1088, 1076, 1035, 942, 858, 753, 614, 535; ^{1}H NMR (500 MHz, $CDCl_3$) δ 10.52 (s, 1H, H-1'), 8.87 (d, $^3J_{4,5}$ 8.1 Hz, 1H, H-4), 7.74 (d, *J* 7.5 Hz, 1H), 7.57 (s, 1H, H-10), 7.51 (t, *J* 7.7 Hz, 1H), 7.29 (d, *J* 7.7 Hz, 1H), 7.12 (t, *J* 7.9 Hz, 2H), 7.02 (t, *J* 7.5 Hz, 1H), 6.99 (d, *J* 8.0 Hz, 1H), 5.16 (s, 2H, H-8 and H-8'), 4.96 (s, 1H, H-1''), 4.71 (d, *J* 5.8 Hz, 1H, H-2''), 4.62 (d, *J* 5.9 Hz, 1H, H-3''), 4.53-4.42 (m, 2H, H-4''and H-5''), 4.36 (dd, *J* 16.0, 9.9 Hz, 1H, H-5''), 3.29 (s, 3H, -OMe), 1.43 (s, 3H, -CH_3), 1.28 (s, 3H, -CH_3); ^{13}C NMR (126 MHz, $CDCl_3$) δ 188.2, 170.4, 151.6, 143.3, 140.5, 139.5, 137.0, 129.4, 125.5, 125.3, 123.0, 122.7, 121.8, 121.1, 120. 5, 113.0, 111.9, 110.1, 109.0, 106.3, 85.0, 85.0, 81.8, 55.6, 53.2, 35.4, 29.7, 26.4, 24.9.

(*Z*)-1'-((1-(((3a*R*,4*R*,6*R*,6a*R*)-6-Methoxy-2,2-dimethyltetrahydrofuro[3,4-*d*][1,3]dioxol-4-yl)methyl)-1*H*-1,2,3-triazol-4-yl)methyl)-[2,3'-biindolinylidene]-2',3-dione (**11**)

IR (ATR) ν /cm^{-1} 3314, 2948, 1712, 1651, 1596, 1468, 1370, 1320, 1210, 1172, 1088, 1018, 858, 742; ^{1}H NMR (500 MHz, $CDCl_3$) δ 10.53 (s, 1H), 8.86 (d, *J* 7.7 Hz, 1H), 7.74 (d, *J* 7.5 Hz, 1H), 7.63 (s, 1H), 7.52 (t, *J* 7.6 Hz, 1H), 7.24 (s, 1H), 7.11 (t, *J* 7.0 Hz, 2H), 7.02 (dd, *J* 15.6, 7.8 Hz, 2H), 5.18 (d, *J* 15.7 Hz, 1H), 5.12 (d, *J* 15.7 Hz, 1H), 4.70 (d, *J* 14.5 Hz, 1H), 4.61 (dd, *J* 7.8, 2.6 Hz, 1H), 4.43 (d, *J* 14.5 Hz, 1H), 4.40 (d, *J* 2.6 Hz, 1H), 4.21 (d, *J* 7.8 Hz, 1H), 3.87 (d, *J* 12.9 Hz, 1H), 3.75 (d, *J* 12.9 Hz, 1H), 1.48 (s, 3H), 1.38 (s, 3H), 1.34 (s, 3H), 0.54 (s, 3H); ^{13}C NMR (126 MHz, $CDCl_3$) δ 188.46, 170.5, 151.7, 143.0, 140.7, 139.7, 137.2, 129. 5, 125.7, 125.5, 125.2, 123.1, 121.9, 121.2, 120.2, 112.1, 109.6, 109.4, 109.2, 106.4, 100.8, 70.7, 70.2, 62.0, 55.0, 35.5, 26.5, 26.1, 24.1, 24.1.

General procedure for hydrophilic indirubin-triazole derivatives (compounds **12-14**)

The hydrolysis reaction was performed by dissolving 0.08 mmol of the intermediates (**9-12**) in THF (2 mL), 0.2 mL of a 9:1 TFA/H_2O v/v solution and 1 drop of concentrated H_2SO_4. The reaction mixture was stirred for 24 h at 60 ºC. The consumption of the starting material was verified by TLC (8:2 ethyl acetate/ethanol) and revealed by 8:2 H_2SO_4/ethanol v/v solution and phosphomolybdic acid. After completion of the reaction, the solvent was dried and the products quickly washed with ethyl ether and stored under an N_2 atmosphere.

1'-[1-(3,4,5,6-Tetrahydroxy-tetrahydro-pyran-2-ylmethyl)-1*H*-[1,2,3]triazol-4-ylmethyl]-1*H*,1'*H*-[2,3']biindolylidene-3,2'-dione (**12**)

^{1}H NMR (400 MHz, DMSO) δ 11.12 (s, 1H), 8.81 (d, *J* 7.7 Hz, 1H), 8.11-8.02 (m, 1H), 7.67 (d, *J* 7.5 Hz, 1H), 7.60 (t, *J* 7.6 Hz, 1H), 7.43 (d, *J* 7.9 Hz, 1H), 7.31 (d, *J* 7.6 Hz, 1H), 7.18 (d, *J* 7.7 Hz, 1H), 7.10-7.01 (m, 2H), 5.41-5.25 (m, 1H), 5.23-5.18 (m, 1H), 5.10 (s, 2H), 4.97-4.92 (m, 1H), 4.87 (d, *J* 2.0 Hz, 1H), 4.49-4.35 (m, 7H), 3.51 (s, 2H), 3.45-3.41 (m, 1H), 3.38 (s, 1H), 3.36-3.27 (m, 3H).

1'-[1-(3,4,5-Trihydroxy-tetrahydro-furan-2-ylmethyl)-1*H*-[1,2,3]triazol-4-ylmethyl]-1*H*,1'*H*-[2,3']biindolylidene-3,2'-dione (**13**)

IR (ATR) ν / cm^{-1} 3297, 292, 2855, 1704, 1651, 1605, 1465, 1073, 748, 576; ^{1}H NMR (500 MHz, DMSO) δ 11.13 (s, 1H), 8.81 (d, *J* 7.7 Hz, 1H), 8.18-7.92 (m, 2H), 7.67 (d, *J* 7.5 Hz, 1H), 7.63-7.55 (m, 1H), 7.43 (d, *J* 7.9 Hz, 1H), 7.31 (s, 2H), 7.14-7.12 (m, 2H), 7.12-7.06 (m, 2H), 7.06-7.01 (m, 2H), 5.12 (s, 2H), 3.55-3.47 (m, 4H), 1.23 (s, 2H); ^{13}C NMR (126 MHz, DMSO) δ 188.6, 168.7, 152.6, 140.8, 138.8, 137.3, 129.1, 124.5, 121.9, 121.5, 120.8, 119.1, 113.5, 109.1, 105.2, 88.8, 79.0, 69.8, 61.1, 34.6.

Difunctionalized-triazole-indirubin (**16**)

The reductive coupling attempt was performed by dissolving (0.261 mmol) of substrate (**15**) in EtOH (2 mL), the reaction mixture was heated to 80 ºC and was then added (0.261 mmol, 1 eq) $NaBH_4$. The reaction was stirred for 2 h, and the color of the solution changed from brown to green and the consumption of the starting material was verified by TLC (7:3 hexane/ethyl acetate). At the end of the reaction the solvent was dried under reduced pressure and the solid purified by column chromatography (9:1 hexane/ethyl acetate).

1,1'-Bis((1-(4-bromophenyl)-1*H*-1,2,3-triazol-4-yl)methyl)-2,3-dihydroxy-[2,3'-biindolin]-2'-one (**16**)

^{1}H NMR (500 MHz, $CDCl_3$) δ 8.21 (s, 2H), 8.06 (s, 2H), 7.93 (dd, *J* 8.0, 1.6 Hz, 1H), 7.85 (s, 1H), 7.61 (ddd, *J* 13.8, 11.7, 7.9 Hz, 24H), 7.37-7.32 (m, 6H), 7.28 (d, *J* 7.3 Hz, 2H), 7.13 (t, *J* 7.5 Hz, 4H), 7.05 (t, *J* 7.6 Hz, 2H), 7.00 (d, *J* 7.7 Hz, 2H), 6.76 (d, *J* 8.0 Hz, 1H), 5.30 (s, 4H), 5.22 (d, *J* 16.1 Hz, 2H), 5.10 (s, 4H), 4.98 (d, *J* 16.0 Hz, 2H), 4.67 (d, *J* 5.9 Hz, 2H), 3.87 (d, *J* 1.7 Hz, 2H), 3.33 (d, *J* 17.6 Hz, 2H), 3.18 (d, *J* 17.4 Hz, 2H), 2.13 (s, 6H); ^{13}C NMR (126 MHz, $CDCl_3$) δ 183.2, 158.6, 150.5, 142.8, 138. 8, 133.0, 132. 9, 130.3, 129.4, 125.5, 124.2, 123.6, 122.8, 122.4, 121.9, 121.1, 117.5, 111.5, 109.9, 35.5, 31.2.

N-Propargylation reaction of indirubin (**19**)

To a round bottom flask, it was added (3.64 mmol, 1.0 eq) of indirubin and solubilized in DMF. Next, (10.92 mmol, 3.0 eq) of propargyl bromide, (10.92 mmol, 3.0 eq) of K_2CO_3, (0.364 mmol, 0.1 eq) KI and (0.364 mmol, 0.1 eq) of triethylammonium bromide were then added according to the methodology of Dan *et al.*[24] The reaction mixture was kept at room temperature for 24 h and the consumption of the starting material was verified by TLC (7:3 hexane/ethyl acetate). After the end of the reaction, the product was extracted with ethyl acetate (3 × 25 mL), the organic phase was dried under reduced pressure and the solid purified by column chromatography (8:2 hexane/ethyl acetate).

1'-Prop-2-ynyl-1*H*,1'*H*-[2,3']biindolylidene-3,2'-dione (**19**)

IR (ATR) ν / cm^{-1} 3288, 3247, 2922, 2852, 1712, 1675, 1611, 1468, 1326, 1192, 1085, 753, 684; ^{1}H NMR (400 MHz, $CDCl_3$) δ 10.49 (s, 1H), 8.92 (d, *J* 7.4 Hz, 1H), 7.75 (d, *J* 7.6 Hz, 1H), 7.55-7.48 (m, 1H), 7.36 (td, *J* 7.7, 1.1 Hz, 1H), 7.18 (td, *J* 7.7, 1.0 Hz, 1H), 7.09 (d, *J* 7.8 Hz, 1H),

7.05-6.99 (m, 2H), 4.64 (d, *J* 2.5 Hz, 2H), 2.26 (t, *J* 2.5 Hz, 1H); ^{13}C NMR (101 MHz, $CDCl_3$) δ 188.4, 169.98, 170.0, 151.7, 140.2, 139.8, 137.2, 129.3, 125.7, 125.5, 123.2, 122.0, 121.4, 120.2, 112.1, 108.9, 77.4, 72.4, 29.9, 29.2.

Theoretical section

The QM calculations were performed with the Gaussian 09 revision D01[42] software. The geometry optimizations were performed with B3LYP[43] functional and 6-31G(d,p)[44] level in DMSO using the polarizable continuum model (PCM). Harmonic frequency calculations were conducted in the same level of theory. Afterwards, some single point energy calculations were carried out to proper obtain the energetic profile for the reaction paths at ωB97XD[45] DFT functional along with 6-311G+(d,p)[44] and SMD[46] solvation method describing DMSO as solvent.

Energy values were calculated according to equation 1 (Gibbs free energy calculation for the species). G_{sol} stands for Gibbs free energy in solution, E_{el} is the SMD/wb97XD/6-311G+(d,p) single point electronic energy, G_{TC} is the thermal correction to the free energy at IEF-PCM/B3LYP/6-31G(d,p) and the 1.89 kcal mol^{-1} is the conversion from 1 atm to 1 mol L^{-1}, in standard state.

$$G_{sol} = E_{el} + G_{TC} + 1.89 \text{ kc al mol}^{-1} \quad (1)$$

Molecular docking

The structures for the Docking analysis were optimized using the semi-empirical method AM1[47] employing the Gaussian 09 D1 revision[42] software package and solvated according to the PCM with water as solvent. Some docking analysis for the compounds in this work was performed employing Autodock 4.2.6 software[48] and visualization software included in Autodock Tools. The GSK-3β enzyme, which is considered a target for the synthesized compounds, was obtained from PDB databank under the code 1Q41. The docking simulations were evaluated for one monomer and the ligand site was defined in the protein based on the complex structure with indirubin present in the original PDB. The space was defined as 18.75 Å edged cube centered in the cartesian coordinates (x, y, z: 40.0, 6.0, 36.5). All docking related settings were kept as default and there were obtained 10 structures for the complex containing the protein and each studied ligand.

Subsequently, the lowest binding energy structure regarding the four best performing dockings for a molecular dynamics study were chosen. The molecular dynamics simulations (MD) were performed in the AMBER 16 software package[49] implementing the GAFF force field[50,51] for the ligands, FF14SB forcefield for the protein residues and water molecules according to the TIP3P model.[52] The simulation protocol consisted of a two-step minimization procedure, alternating heating and equilibrium steps and finally a production simulation. The first minimization consisted of 1000 steepest descent cycles followed by using 1500 conjugated gradients approach keeping the solute restraint by applying a restraint force constant of 500 kcal mol^{-1} Å^{-2}. Differently from the first minimization, the second followed the very same conditions but restraining the solute, leaving the entire complex to minimize. There were 6 heating-equilibrium, which the first 5 increased the temperature in 50 K comprising 2 fs in constant volume periodic boundaries (NVT) (2800 cycles) followed by 2 fs of equilibrium (5000 frames) using constant pressure periodic boundary (NPT) with a pressure mean of 1 bar. The last step increased the temperature in 60 K along with a 10000 frames equilibrium step (4 fs) both with the same protocol as before.

The production stage comprised of 100 ns, with 2 fs long increases in time, applying NPT with temperatures kept around 310 K implementing Langevin thermostat[53] and pressure around 1 bar with Berendsen barostat.[54] The SHAKE algorithm was implemented to restraint the hydrogen stretching movement in the molecules and all non-bonded interactions were settled with a cut-off distance of 6.0 Å. Although the productions were 100 ns long only the last 50 ns of each was taken for analysis due to the thermodynamic stability of the systems.

Afterwards, several analyses were conducted based on the trajectories. The RMSD calculates the atomic deviation based on an initial reference, which was the first frame in this work (equation 2). In addition, a SASA analysis was also accounted for each system. The SASA calculation consists of a sum of the available area in the protein to the solvent, and thus, to other solutes in the aqueous environment.

$$\text{RMSD} = \sqrt{\frac{\sum_{i=0}^{N}[m_i * \left(X_i - Y_i^2\right)}{M}} \quad (2)$$

where i is an specific atom, m_i is the mass of the atom, X_i represents atomic coordinates of I and Y_i represents the atomic coordinates of I in the reference structure. M is the total mass of the system.

Supplementary Information

Supplementary information (copies of NMR spectra and theoretical data) is available free of charge at http://jbcs.sbq.org.br as PDF file.

Acknowledgements

We are grateful for generous financial support from CAPES (Finance Code 001), CNPq, FAPEMIG, UFJF, EULER-CeMEAI/USP and Rede Mineira de Química.

Author Contributions

A. F. S. Fuzaro was responsible for experimental investigation, data curation; F. H. C. Ferreira for theoretical investigation and writing; G. L. P. Suhett for experimental investigation; L. A. S. Costa for theoretical investigation and revision; R. M. Grazul for revision and experimental advice; M. V. de Almeida for conceptualization, formal analysis funding acquisition, project administration and revision; E. P. Ávila for data curation, theoretical investigation, writing and revision.

References

1. Yang, L.; Li, X.; Huang, W.; Rao, X.; Lai, Y.; *Biomed. Pharmacother.* **2022**, *151*, 113112. [Crossref]
2. Tu, P.; Tian, R.; Lu, Y.; Zhang, Y.; Zhu, H.; Ling, L.; Li, H.; Chen, D.; *Chin. Med.* **2020**, *15*, 128. [Crossref]
3. Zhang, A.; Yu, M.; Lan, T.; Liu, Z.; Mao, Z.; *Synth. Commun.* **2010**, *40*, 3125. [Crossref]
4. Sethi, G.; Ahn, K. S.; Sandur, S. K.; Lin, X.; Chaturvedi, M. M.; Aggarwal, B. B.; *J. Biol. Chem.* **2006**, *281*, 23425. [Crossref]
5. Moon, M. J.; Lee, S. K.; Lee, J.-W.; Song, W. K.; Kim, S. W.; Il Kim, J.; Cho, C.; Choi, S. J.; Kim, Y.-C.; *Bioorg. Med. Chem.* **2006**, *14*, 237. [Crossref]
6. Zhu, J.; Langer, P.; Ulrich, C.; Eberle, J.; *Antioxidants* **2021**, *10*, 1514. [Crossref]
7. Magiatis, P.; Polychronopoulos, P.; Skaltsounis, A.-L.; Lozach, O.; Meijer, L.; Miller, D. B.; O'Callaghan, J. P.; *Neurotoxicol. Teratol.* **2010**, *32*, 212. [Crossref]
8. Jung, H.-J.; Nam, K. N.; Son, M.-S.; Kang, H.; Hong, J.-W.; Kim, J. W.; Lee, E. H.; *Neurosci. Lett.* **2011**, *487*, 139. [Crossref]
9. Ju, Z.; Sun, J.; Liu, Y.; *Molecules* **2019**, *24*, 3831. [Crossref]
10. Ginzinger, W.; Egger, A.; Mühlgassner, G.; Arion, V. B.; Jakupec, M. A.; Galanski, M. S.; Berger, W.; Keppler, B. K.; *Chem. Biodiversity* **2012**, *9*, 2175. [Crossref]
11. Sun, B.; Wang, J.; Liu, L.; Mao, L.; Peng, L.; Wang, Y.; *Chem. Biol. Drug Des.* **2021**, *97*, 565. [Crossref]
12. Kolb, H. C.; Sharpless, K. B.; *Drug Discovery Today* **2003**, *8*, 1128. [Crossref]
13. Manna, T.; Pal, K.; Jana, K.; Misra, A. K.; *Bioorg. Med. Chem. Lett.* **2019**, *29*, 126615. [Crossref]
14. Agalave, S. G.; Maujan, S. R.; Pore, V. S.; *Chem. - Asian J.* **2011**, *6*, 2696. [Crossref]
15. Lauria, A.; Delisi, R.; Mingoia, F.; Terenzi, A.; Martorana, A.; Barone, G.; Almerico, A. M.; *Eur. J. Org. Chem.* **2014**, *2014*, 3289. [Crossref]
16. Dunn, G. L.; Hoover, J. R. E.; Berges, D. A.; Taggart, J. J.; Davis, L. D.; Dietz, E. M.; Jakas, D. R.; Yim, N.; Actor, P.; Uri, J. V.; Weisbach, J. A.; *J. Antibiot.* **1976**, *29*, 65. [Crossref]
17. Yang, Y.; Rasmussen, B. A.; Shlaes, D. M.; *Pharmacol. Ther.* **1999**, *83*, 141. [Crossref]
18. Alam, M. M.; *Arch. Pharm.* **2022**, *355*, 2100158. [Crossref]
19. Obafemi, C. A.; Adegbite, O. B.; Fadare, O. A.; Iwalewa, E. O.; Omisore, N. O.; Sanusi, K.; Yilmaz, Y.; Ceylan, Ü.; *Heliyon* **2021**, *7*, e05756. [Crossref]
20. Brandão, P.; Pinheiro, D.; de Melo, J. S. S.; Pineiro, M.; *Dyes Pigm.* **2020**, *173*, 107935. [Crossref]
21. Wang, C.; Yan, J.; Du, M.; Burlison, J. A.; Li, C.; Sun, Y.; Zhao, D.; Liu, J.; *Tetrahedron* **2017**, *73*, 2780. [Crossref]
22. Riepl, H. M.; Urmann, C.; *Helv. Chim. Acta* **2012**, *95*, 1461. [Crossref]
23. Ferandin, Y.; Bettayeb, K.; Kritsanida, M.; Lozach, O.; Polychronopoulos, P.; Magiatis, P.; Skaltsounis, A.-L.; Meijer, L.; *J. Med. Chem.* **2006**, *49*, 4638. [Crossref]
24. Dan, N. T.; Quang, H. D.; Van Truong, V.; Huu Nghi, D.; Cuong, N. M.; Cuong, T. D.; Toan, T. Q.; Bach, L. G.; Anh, N. H. T.; Mai, N. T.; Lan, N. T.; Van Chinh, L.; Quan, P. M.; *Sci. Rep.* **2020**, *10*, 11429. [Crossref]
25. Kolb, H. C.; Finn, M. G.; Sharpless, K. B.; *Angew. Chem.* **2001**, *113*, 2056. [Crossref]
26. de Souza, R. O. M. A.; e Miranda, L. S. M.; *An. Acad. Bras. Cienc.* **2019**, *91*, e20180751. [Crossref]
27. Worrell, B. T.; Malik, J. A.; Fokin, V. V.; *Science* **2013**, *340*, 457. [Crossref]
28. Varun, V.; Sonam, S.; Kakkar, R.; *MedChemComm* **2019**, *10*, 351. [Crossref]
29. Nath, R.; Pathania, S.; Grover, G.; Akhtar, M. J.; *J. Mol. Struct.* **2020**, *1222*, 128900. [Crossref]
30. Tri, N. M.; Thanh, N. D.; Ha, L. N.; Anh, D. T. T.; Toan, V. N.; Giang, N. T. K.; *Chem. Pap.* **2021**, *75*, 4793. [Crossref]
31. Ullrich, R.; Poraj-Kobielska, M.; Herold-Majumdar, O. M.; Vind, J.; Hofrichter, M.; *Catalysts* **2021**, *11*, 1495. [Crossref]
32. Ferreira, J. T.; Pina, J.; Ribeiro, C. A. F.; Fernandes, R.; Tomé, J. P. C.; Rodríguez-Morgade, M. S.; Torres, T.; *Chem. - A Eur. J.* **2020**, *26*, 1789. [Crossref]
33. Libnow, S.; Methling, K.; Hein, M.; Michalik, D.; Harms, M.; Wende, K.; Flemming, A.; Köckerling, M.; Reinke, H.; Bednarski, P. J.; Lalk, M.; Langer, P.; *Bioorg. Med. Chem.* **2008**, *16*, 5570. [Crossref]
34. Jacobs, K. M.; Bhave, S. R.; Ferraro, D. J.; Jaboin, J. J.; Hallahan, D. E.; Thotala, D.; *Int. J. Cell Biol.* **2012**, *2012*, ID 930710. [Crossref]
35. Frame, S.; Cohen, P.; *Biochem. J.* **2001**, *359*, 1. [Crossref]
36. Doble, B. W.; Woodgett, J. R.; *J. Cell Sci.* **2003**, *116*, 1175. [Crossref]
37. Luo, J.; *Cancer Lett.* **2009**, *273*, 194. [Crossref]

38. Selenica, M.; Jensen, H. S.; Larsen, A. K.; Pedersen, M. L.; Helboe, L.; Leist, M.; Lotharius, J.; *Br. J. Pharmacol.* **2007**, *152*, 959. [Crossref]
39. Bertrand, J. A.; Thieffine, S.; Vulpetti, A.; Cristiani, C.; Valsasina, B.; Knapp, S.; Kalisz, H. M.; Flocco, M.; *J. Mol. Biol.* **2003**, *333*, 393. [Crossref]
40. Junior, C. O. R.; Castro, S. B. R.; Pereira, A. A.; Alves, C. C. S.; Oliveira, E. E.; Rêgo, R. T.; Ferreira, A. P.; de Almeida, M. V.; *Eur. J. Med. Chem.* **2014**, *85*, 615. [Crossref]
41. Muraca, A. C. A.; Raminelli, C.; *ACS Omega* **2020**, *5*, 2440. [Crossref]
42. Frisch, M. J.; Trucks, G. W.; Schlegel, H. B.; Scuseria, G. E.; Robb, M. A.; Cheeseman, J. R.; Scalmani, G.; Barone, V.; Mennucci, B.; Petersson, G. A.; Nakatsuji, H.; Caricato, M.; Li, X.; Hratchian, H. P.; Izmaylov, A. F.; Bloino, J.; Zheng, G.; Sonnenberg, J. L.; Hada, M.; Ehara, M.; Toyota, K.; Fukuda, R.; Hasegawa, J.; Ishida, M.; Nakajima, T.; Honda, Y.; Kitao, O.; Nakai, H.; Vreven, T.; Montgomery, J. A. J.; Peralta, J. E.; Ogliaro, F.; Bearpark, M.; Heyd, J. J.; Brothers, E.; Kudin, K. N.; Staroverov, V. N.; Keith, T.; Kobayashi, R.; Normand, J.; Raghavachari, K.; Rendell, A.; Burant, J. C.; Iyengar, S. S.; Tomasi, J.; Cossi, M.; Rega, N.; Millam, J. M.; Klene, M.; Knox, J. E.; Cross, J. B.; Bakken, V.; Adamo, C.; Jaramillo, J.; Gomperts, R.; Stratmann, R. E.; Yazyev, O.; Austin, A. J.; Cammi, R.; Pomelli, C.; Ochterski, J. W.; Martin, R. L.; Morokuma, K.; Zakrzewski, V. G.; Voth, G. A.; Salvador, P.; Dannenberg, J. J.; Dapprich, S.; Daniels, A. D.; Farkas, O.; Foresman, J. B.; Ortiz, J. V.; Cioslowski, J.; Fox, D. J.; *Gaussian 09*, revision D.01; Gaussian Inc.: Wallingford CT, 2013.
43. Becke, A. D.; *J. Chem. Phys.* **1993**, *98*, 5648. [Crossref]
44. Ditchfield, R.; Hehre, W. J.; Pople, J. A.; *J. Chem. Phys.* **1971**, *54*, 724. [Crossref]
45. Chai, J.-D.; Head-Gordon, M.; *J. Chem. Phys.* **2008**, *128*, 84106. [Crossref]
46. Marenich, A. V; Cramer, C. J.; Truhlar, D. G.; *J. Phys. Chem. B* **2009**, *113*, 6378. [Crossref]
47. Dewar, M. J. S.; Zoebisch, E. G.; Healy, E. F.; Stewart, J. J. P.; *J. Am. Chem. Soc.* **1985**, *107*, 3902. [Crossref]
48. Morris, G. M.; Huey, R.; Lindstrom, W.; Sanner, M. F.; Belew, R. K.; Goodsell, D. S.; Olson, A. J.; *J. Comput. Chem.* **2009**, *30*, 2785. [Crossref]
49. Case, D. A.; Betz, R. M.; Cerutti, D. S.; Cheatham III, T. E.; Darden, T. A.; Duke, R. E.; Giese, T. J.; Gohlke, H.; Goetz, A. W.; Homeyer, N.; *Amber* 16; University of California: San Francisco, 2016. [Crossref]
50. Wang, J.; Wang, W.; Kollman, P. A.; Case, D. A.; *J. Mol. Graphics Modell.* **2006**, *25*, 247. [Crossref]
51. Wang, J.; Wolf, R. M.; Caldwell, J. W.; Kollman, P. A.; Case, D. A.; *J. Comput. Chem.* **2004**, *25*, 11457. [Crossref]
52. Pálinkás, G.; Kálmán, E.; Kovács, P.; *Mol. Phys.* **1977**, *34*, 525. [Crossref]
53. Uberuaga, B. P.; Anghel, M.; Voter, A. F.; *J. Chem. Phys.* **2004**, *120*, 6363. [Crossref]
54. Berendsen, H. J. C.; Postma, J. P. M.; Van Gunsteren, W. F.; Dinola, A.; Haak, J. R.; *J. Chem. Phys.* **1984**, *81*, 3684. [Crossref]

Submitted: May 31, 2023
Published online: September 27, 2023